PNAS RESEARCH ARTICLE | ENGINEERING

Regulating the reduction reaction pathways via manipulating the solvation shell and donor number of the solvent in Li-CO_2 chemistry

Wenchao Zhang[a,b,1], Fangli Zhang[c,1], Sailin Liu[d], Wei Kong Pang[c], Zhang Lin[a,b,2], Zaiping Guo[d,2], and Liyuan Chai[a,b]

Edited by Alexis Bell, University of California, Berkeley, CA; received November 18, 2022; accepted February 6, 2023

Transforming CO_2 into valuable chemicals is an inevitable trend in our current society. Among the viable end-uses of CO_2, fixing CO_2 as carbon or carbonates via Li-CO_2 chemistry could be an efficient approach, and promising achievements have been obtained in catalyst design in the past. Even so, the critical role of anions/solvents in the formation of a robust solid electrolyte interphase (SEI) layer on cathodes and the solvation structure have never been investigated. Herein, lithium bis(trifluoromethanesulfonyl)imide (LiTFSI) in two common solvents with various donor numbers (DN) have been introduced as ideal examples. The results indicate that the cells in dimethyl sulfoxide (DMSO)-based electrolytes with high DN possess a low proportion of solvent-separated ion pairs and contact ion pairs in electrolyte configuration, which are responsible for fast ion diffusion, high ionic conductivity, and small polarization. The 3 M DMSO cell delivered the lowest polarization of 1.3 V compared to all the tetraethylene glycol dimethyl ether (TEGDME)-based cells (about 1.7 V). In addition, the coordination of the O in the $TFSI^-$ anion to the central solvated Li^+ ion was located at around 2 Å in the concentrated DMSO-based electrolytes, indicating that $TFSI^-$ anions could access the primary solvation sheath to form an LiF-rich SEI layer. This deeper understanding of the electrolyte solvent property for SEI formation and buried interface side reactions provides beneficial clues for future Li-CO_2 battery development and electrolyte design.

solid electrolyte interphase | solvation shell | donor number | electrolyte engineering | Li-CO_2 batteries

Significance

Li-CO_2 chemistry is an efficient approach for fixing CO_2, and promising achievements have been obtained in catalyst design/electrolyte engineering. Even so, the critical role of anions/solvents in the formation of a robust solid electrolyte interphase (SEI) layer on cathodes and the solvation structure have never been investigated. This work introduces LiTFSI in TEGDME and DMSO as solvents with different donor numbers (DNs) as ideal examples to systematically study the effect of solvents and salt concentrations on the electrochemical performance of Li-CO_2 cells. The results may deepen our understanding of anions/solvents in the formation of the SEI and offer an insight into better interphase design for future electrolyte engineering in Li-CO_2 chemistry.

Carbon dioxide (CO_2), as one of the leading greenhouse gases, has been attracting great attention in the context of global climate change (1). Transforming CO_2 into other chemicals is an inevitable trend, but it requires a large energy input and might cause further environmental pollution to some extent (2–4). In addition, various products such as methane or formic acid require an extra compression or liquefaction process for storage and transport, which gives rise to additional energy consumption. Hence, realizing an effective approach to fix CO_2 such as in carbon or carbonates is the future trend in our current society. Li-CO_2 batteries have also attracted considerable attention due to their high energy density (1,879 Wh/kg) and relatively high discharge potential (~2.8 V) (5, 6). In addition, CO_2 gas is highly soluble in organic solvents and prone to react with intermediate superoxide radicals, which makes Li-CO_2 chemistry favorable in metal–gas batteries.

Currently, Li-CO_2 chemistry is facing numerous challenges, such as unstable solid electrolyte interphase (SEI) layers on cathodes, sluggish ion diffusivity, and high CO_2 evolution reaction (CER) polarization potential (7). Although various solid catalysts have been widely studied for promoting the CO_2 reduction reaction and CER as well as improving energy efficiency, the unclear dynamics of the formation of the SEI in organic electrolytes have largely hindered the optimization of suitable electrolytes for the future (8–10). The past few years have witnessed the successful application of aprotic electrolytes containing ether or sulfone solvents in metal–CO_2 batteries. Among them, TEGDME and DMSO are two widely accepted solvents in Li-CO_2 batteries. To the best of our knowledge, most studies have focused on the performance evaluation of these two electrolyte solvents in terms of their optimized catalysts, but they have barely initiated studies leading to any fundamental understanding of the roles of anions and solvents at the electrode/electrolyte interface. The discharge reaction pathways include the "surface reaction pathway" and the "solvent reaction pathway," which generally govern the formation of the SEI layer in Li-CO_2 batteries. The discharge products of Li_2CO_3 form via a direct reaction of free Li^+ and CO_3^{2-} on the cathode surface through the surface reaction pathway, showing fast reaction kinetics but not forming protective SEI layers. In contrast, solvated Li^+ ions as the key intermediate can transform the dissolved CO_2 into Li_2CO_3 in electrolytes after desolvation, and then deposit it on the cathode surface via the solvent reaction pathway,

Author contributions: W.Z. and Z.G. designed research; W.Z. performed research; S.L., W.K.P., Z.L., and L.C. contributed new reagents/analytic tools; F.Z. analyzed data; and F.Z. and Z.G. wrote the paper.

The authors declare no competing interest.

This article is a PNAS Direct Submission.

[1]W.Z. and F.Z. contributed equally to this work.

[2]To whom correspondence may be addressed. Email: zhang_lin@csu.edu.cn or zaiping.guo@adelaide.edu.au.

This article contains supporting information online at https://www.pnas.org/lookup/suppl/doi:10.1073/pnas.2219692120/-/DCSupplemental.

Published March 30, 2023.

which is beneficial to SEI formation (11). Nevertheless, either the surface or the solvent reaction pathway dominates the main discharge reduction pathway, and the critical role of solvents in various electrolytes is still a mystery in Li-CO_2 batteries.

To address the challenges of the unstable SEI layer and the large polarization in Li-CO_2 chemistry, in this work, we initiated systematic studies of the chemical properties of the electrolytes, the anion role of concentrated bis(trifluoromethanesulfonyl)imide ($TFSI^-$), and the role of the solvation shell on the formation of SEI layer. In addition, highly concentrated electrolyte, which is regarded as a cost-effective and pragmatic approach, was employed to address the parasitic reactions between the electrolyte and the electrodes, which has not been realized in Li-CO_2 batteries as yet (12, 13). Herein, we discovered that the TEGDME solvent with a low donor number (DN) (DN = 16.6 kcal mol^{-1}) possesses a much higher proportion of solvent-separated ion pairs (SSIPs) and contact ion pairs (CIPs) structure than that in DMSO solvent with a high DN (DN = 29.8 kcal mol^{-1}) (14, 15). As a result, DMSO-based electrolytes within a concentration range from 0.5 M to 4 M could all lead to faster Li^+ ion diffusion kinetics and thus a lower polarization potential than those in TEGDME-based electrolytes. In addition, benefiting from the high concentration approach, 3 M DMSO electrolyte could lead to higher content of LiF component in the SEI and yield more satisfactory cycling performance than 3 M TEGDME electrolyte, as illustrated in Fig. 1*A*. This work not only reveals the importance of electrolyte solvent properties for the SEI formation and the mechanism of side reactions on the electrode surface, but also will provide guidance for improving the performance of Li-CO_2 batteries through manipulating the solvation structure.

Results and Discussion

In addition to high ionic conductivity and low overpotential, DMSO solvent shows its advantages of low cost, low viscosity, and weak volatility, which are beneficial to industrial application, excellent rate

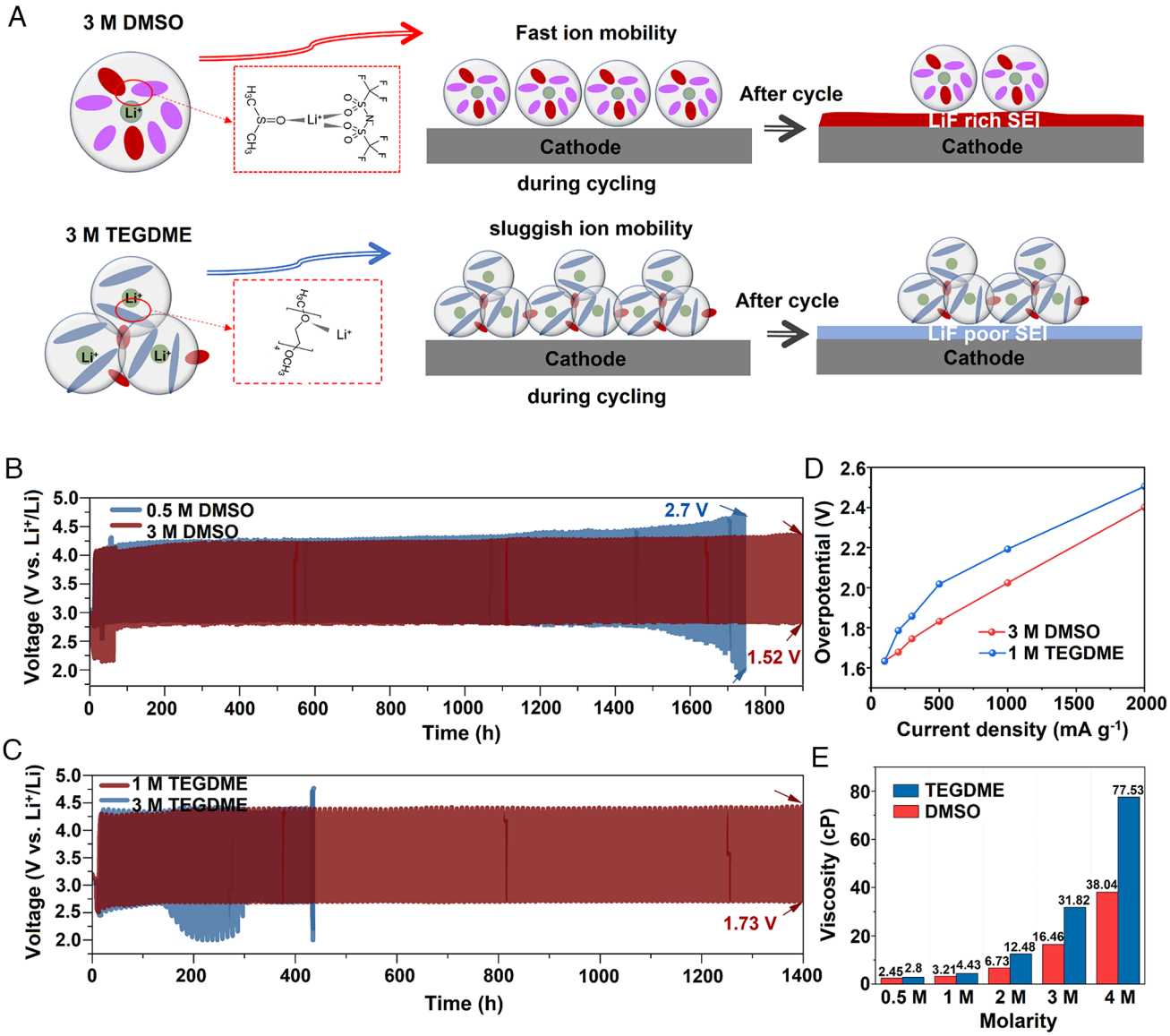

Fig. 1. Electrochemical performances of Li-CO_2 cells. (*A*) Schematic illustrations of the solvation structure and SEI formation on the cathode surface in 3 M DMSO- and 3 M TEGDME-based electrolytes, respectively. (The purple, blue, and red symbols represent the DMSO solvent molecules, the TEGDME solvent molecules, and the $TFSI^-$ anions, respectively.) The voltage–time profiles of the cells at 100 mA g^{-1} with a 500 mA h g^{-1} cut-off specific capacity in (*B*) 0.5 M DMSO- and 3 M DMSO-based electrolytes; and (*C*) 1 M TEGDME- and 3 M TEGDME-based electrolytes. (*D*) Comparison of the polarization potential of the cells in 3 M DMSO- and 1 M TEGDME-based electrolytes at different current densities. (*E*) Viscosity changes of the electrolytes from 0.5 M to 4 M concentrations of DMSO- and TEGDME-based electrolytes under increasing shear rate.

performance, and battery safety (as summarized in *SI Appendix*, Fig. S1). The cycling performance and polarization potential of Li-CO_2 batteries employing DMSO or TEGDME solvents in various LiTFSI-based concentrated electrolytes were evaluated by limiting the cut-off specific capacity to 500 mA h g^{-1}. As shown in *SI Appendix*, Fig. S2, the cell with 3 M LiTFSI in DMSO electrolyte could deliver the lowest overpotential (1.3 V) at 100 mA g^{-1} compared with the other concentrations (0.5 M, 1 M, 2M, 4 M) in 40 cycles. The detailed voltage–time profiles show that the overpotential of the 0.5 M DMSO cell notably increased to 2.7 V after 1,700 h of cycling, whereas, the 3 M DMSO cell maintained a stable and low overpotential of around 1.52 V after 1,900 h (180 cycles) of cycling (Fig. 1*B*). As shown in *SI Appendix*, Fig. S3, the cells with 1 M and 2 M LiTFSI in TEGDME electrolytes delivered relatively lower overpotential compared to the other concentrations (0.5 M, 3 M, 4 M). The 1 M TEGDME cell performed prolonged cycling of 1,400 h with a stable overpotential of 1.73 V, better than for the 3 M TEGDME cell, which just exhibited 430 h of cycling (Fig. 1*C*). For these two types of solvents, the above results revealed that the batteries using DMSO-based electrolytes could offer relatively stable cycling performances and smaller polarization than those of the TEGDME-based electrolytes (*SI Appendix*, Fig. S4). Among the various concentrations, the cells in 3 M DMSO- and 1 M TEGDME-based electrolytes exhibited the best cycling performance. Meanwhile, although the 3 M DMSO electrolyte possesses a higher salt concentration, the polarization potential of the 3 M DMSO cell was much lower than that of the 1 M TEGDME cell (*SI Appendix*, Fig. S5).

The rate capabilities of the Li-CO_2 batteries in DMSO and TEGDME-based electrolytes were evaluated under various concentrations. As shown in *SI Appendix*, Figs. S6 and S7, the cells could deliver flat charge/discharge plateaus with a cut-off 500 mA h g^{-1} specific capacity when the current density was increased from 100 to 2,000 mA g^{-1} under 1 M, 2 M, or 3 M of LiTFSI in the two solvents and 0.5 M in DMSO-based electrolyte. At 1,000 and 2,000 mA g^{-1}, the cell in 0.5 M TEGDME-based electrolyte could only deliver 435 and 314 mA h g^{-1}, respectively. On increasing the salt concentration to 4 M, the capacity could not reach 500 mA h g^{-1} with large polarization at the current densities of 1,000 and 2,000 mA g^{-1} in these two solvents, which might be attributed to the increased viscosity and reduced ionic conductivity of the electrolytes at high salt concentrations. To summarize, the cells in DMSO-based electrolytes showed lower overpotential and superior rate capability compared with the cells in TEGDME-based electrolytes (Fig. 1*D* and *SI Appendix*, Fig. S8). The polarization disparity between the two electrolytes could be reflected to some extent by their viscosity and ionic conductivity. As shown in Fig. 1*E* and *SI Appendix*, Figs. S9 and S10, the LiTFSI in DMSO solvent exhibited much lower viscosity than its counterparts in TEGDME solvent at the same concentrations. The viscosity of 4 M TEGDME electrolyte was 77.53 cp, which is about two times that of 4 M DMSO electrolyte (38.04 cp). The viscosity results indicated that the DMSO-based electrolytes featured high ionic conductivities and fast ion transportation kinetics in liquids (16).

The above results demonstrate that employing the high DN solvent DMSO could effectively reduce the polarization and promote ion diffusion kinetics in electrolytes. The superior electrochemical performances of DMSO compared to TEGDME electrolytes are possibly attributable to the distinct reaction pathways that are derived from different electrolyte solvation structures. The detailed solvent reaction pathways lead to distinct types of SEI formation on the cathode, which influences the reversibility of the intermediate and final products on the cathode, as further revealed with the surface analysis and modeling results discussed below.

The cycling stability and rate capability were governed by the chemical components/structure of the electrode/electrolyte interphase, which could be achieved by manipulating the salt concentrations of electrolytes (17). X-ray photoelectron spectroscopy (XPS) was conducted to examine the possible chemical compositions of SEI products derived from the decomposition of the salt and solvents during electrochemical cycling. The top surface of the cycled cathode consisted of both organic (C–F, C–S, C–O) and inorganic (LiF, Li_2SO_3, Li_2SO_4) components. As shown in Fig. 2 *A* and *C*, the cycled cathodes in DMSO-based electrolytes exhibited higher LiF content in the SEI than those in TEGDME-based electrolytes. Specifically, 13.16% LiF in the SEI could be detected in 3 M DMSO electrolyte on the surface of cathode, which is significantly higher than those in other electrolytes in this work (as calculated from the survey scan, *SI Appendix*, Figs. S11 and S12). Consistent with the XPS results, the largest amount of F on the cycled cathode was detected in the 3 M DMSO electrolyte by energy-dispersive spectroscopy element analysis (*SI Appendix*, Figs. S13 and S14 and Table S1). Similar trends in terms of the variations of inorganic sulfate (Li_2SO_3, Li_2SO_4) with the increased concentration of the salt in the electrolytes could be found in the S 2p spectra, which could be deconvoluted into SO_3^{2-}, SO_4^{2-}, and C–S (Fig. 2*B*) (18). Interestingly, no C–S peak can be detected in the 3 M DMSO cell, indicating that few DMSO molecules could be decomposed. The peak of SO_4^{2-} in 3M DMSO electrolyte shows the strongest intensity compared with those in other electrolytes, demonstrating the highest content of SO_4^{2-} as shown in Fig. 2*D*. Therefore, it could be speculated that the contents of LiF and Li_2SO_4 might be the main components that are crucial to governing the cycling stability in Li-CO_2 batteries (19).

The ex-situ X-ray diffraction patterns (*SI Appendix*, Fig. S15) and the *ex-situ* scanning electron microscope (SEM) images for the pristine cathode and the discharged cathodes in DMSO-based electrolytes (*SI Appendix*, Fig. S16) and TEGDME-based electrolytes (*SI Appendix*, Fig. S17) were taken to verify the formation of Li_2CO_3 as the main discharge products from CO_2 reduction. The C 1s spectra (*SI Appendix*, Figs. S18 and S19) may further reveal the decomposition process and side products from $TFSI^-$ anions and solvent molecules during charge-discharge. The C–C (≈284.5 eV) and C–O (≈285 eV) peaks are ascribed to nonoxygenated ring carbon and oxygen in r-GO catalyst. After recharging, the appearance of C–O–C (≈286.5 eV) and O–C=O (≈288.3 eV) and relatively stronger intensity of these two peaks in TEGDME-based electrolytes suggest that more TEGDME was probably involved in the SEI formation process than DMSO, resulting in electrolyte depletion. It is also worth mentioning that the two peaks corresponding to the CF_2 and CF_3 bonds at around 292 eV and 293 eV show stronger intensity in TEGDME-based electrolytes than those in DMSO-based electrolytes, indicating that the decomposition of $TFSI^-$ anions is prone to form LiF at the cathode/electrolyte interface in DMSO-based electrolytes (20, 21). In high salt concentration electrolytes, the peak intensities of C–O–C, CF_2, and CF_3 kept a notably low level in 3 M DMSO electrolyte compared with 4 M DMSO electrolyte. Since the SEI originates from the decomposition of the solvent and the $TFSI^-$ anions during cycling, which highly depends on the solvation structure, it is critical to determine the differences in SEI formation through analyzing the solvation of different components with Li^+ ions. Therefore, the analysis of the solvation shell structure and validation of the molecular dynamics approach will be discussed next (22).

Since the formation of the SEI is determined by the coordination environment of Li^+ ions, which can lead to different interfacial

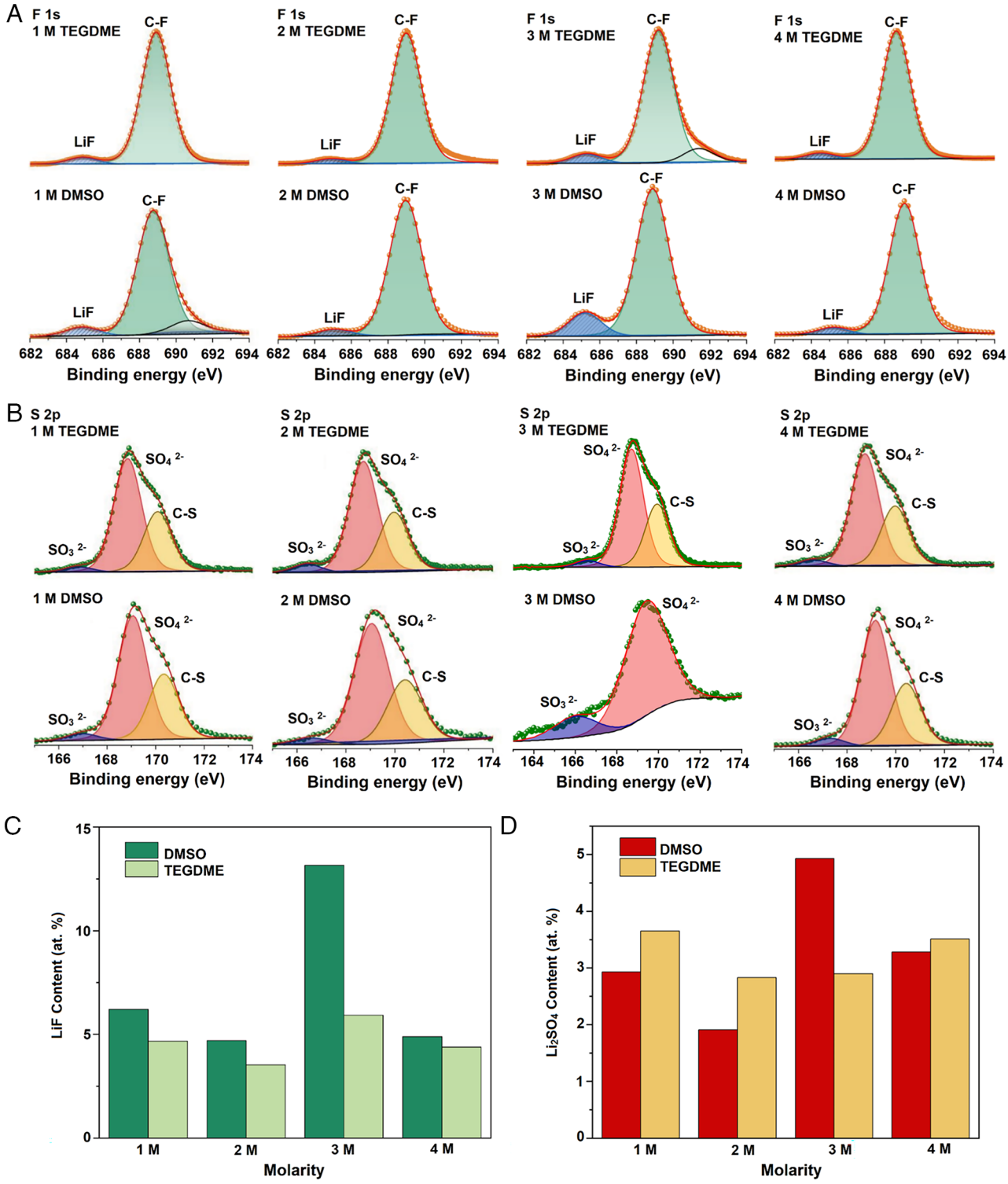

Fig. 2. Characterization of SEI components on cathodes after cycling. XPS fitting curves of (*A*) F 1s and (*B*) S 2p peaks from the cathodes in DMSO- and TEGDME-based electrolytes with various salt concentrations after five cycles at 100 mA g^{-1}. Comparison of (*C*) LiF and (*D*) Li_2SO_4 content on the surfaces of the cathodes after five cycles in various concentrations of DMSO- and TEGDME-based electrolytes.

decomposition behavior (23, 24), Raman spectroscopy and density functional theory (DFT) calculations were jointly employed to reveal the solvation structure and electrolyte configuration of the DMSO and TEGDME-based electrolytes. *SI Appendix*, Figs. S20 and S21 show Raman spectra between 200 and 1,800 cm^{-1} of pure DMSO and TEGDME solutions. New peaks were observed in 3 M DMSO and 1 M TEGDME electrolytes (Fig. 3*A*), corresponding to the addition of LiTFSI (20, 25, 26). As shown in Fig. 3*B*, the peaks located at 667 and 697 cm^{-1} are from the vibrations of C–S symmetric and asymmetric stretching modes from DMSO, respectively. A new peak at 742 cm^{-1} that represents the $TFSI^-$ anion expansion–contraction normal mode of vibration appeared when the salt was introduced into the DMSO solvent. With the addition of LiTFSI at various concentrations, the peaks corresponding to these vibrations became weak. Notably, two new solvated peaks can be observed at 676 and 708 cm^{-1}, which are

assigned to the C–S symmetric and asymmetric stretching modes of DMSO molecules that were solvated with Li^+ ions (27). The above results indicate that the coordination of Li^+ with DMSO becomes stronger with the increased salt concentration. The C–O–C stretching vibration from free TEGDME that was initially located at ~850 cm^{-1} became less intense, while the solvated TEGDME peak (870 cm^{-1}) became more enhanced with increasing salt concentration. These results indicate that the solvation ratio of Li^+ with TEGDME molecules increases with the increased salt concentration in TEGDME-based electrolytes. The solvation ratio of DMSO/TEGDME with Li^+ can be calculated through the Raman fitting curve using the Irish method. As shown in Fig. 3*C*, the ratio of solvated DMSO molecules in concentrated electrolytes could reach as high as 73% and 79% at 3M and 4M concentrations, respectively, which indicated that most DMSO molecules are properly coordinated with Li^+ and that only a few free DMSO molecules exist in the concentrated electrolyte. It should be noted that the solvation ratio in TEGDME solution is lower than that in DMSO solution at all concentrations, indicating more severe side reactions from free TEGDME solvent molecules.

As illustrated in Fig. 1*A*, the electrolyte configuration and the solvation structure in the first solvation shell of single-solvated Li^+ cations are the critical properties that dictate the detailed reaction kinetics via the solvent reaction pathway, since the solvated Li^+ ion is the key intermediate in reaction processes. Specifically, the electrolyte configuration can play an important role in the ion diffusion and the surrounding environment around solvated Li^+ ions in electrolytes, which can be classified as free anions, SSIP-dominated structures, CIP-dominated structures, or aggregating ion pair (AGG)-dominated structures (28). To better evaluate the interaction between Li^+ and $TFSI^-$, various $TFSI^-$ ion pairs were defined by C–N–C bending vibration positions, as shown in Fig. 3*D*. The peaks located at 736 to 738 cm^{-1}, 740 to 742 cm^{-1}, 744 to 746 cm^{-1}, and 746.5 to 747.3 cm^{-1} could be attributed to free $TFSI^-$, SSIPs, CIPs, and ion aggregates (AGGs), respectively (29, 30). The higher proportions of SSIPs and CIPs in the low DN solvent (TEGDME) than those in the high DN solvent (DMSO) at the

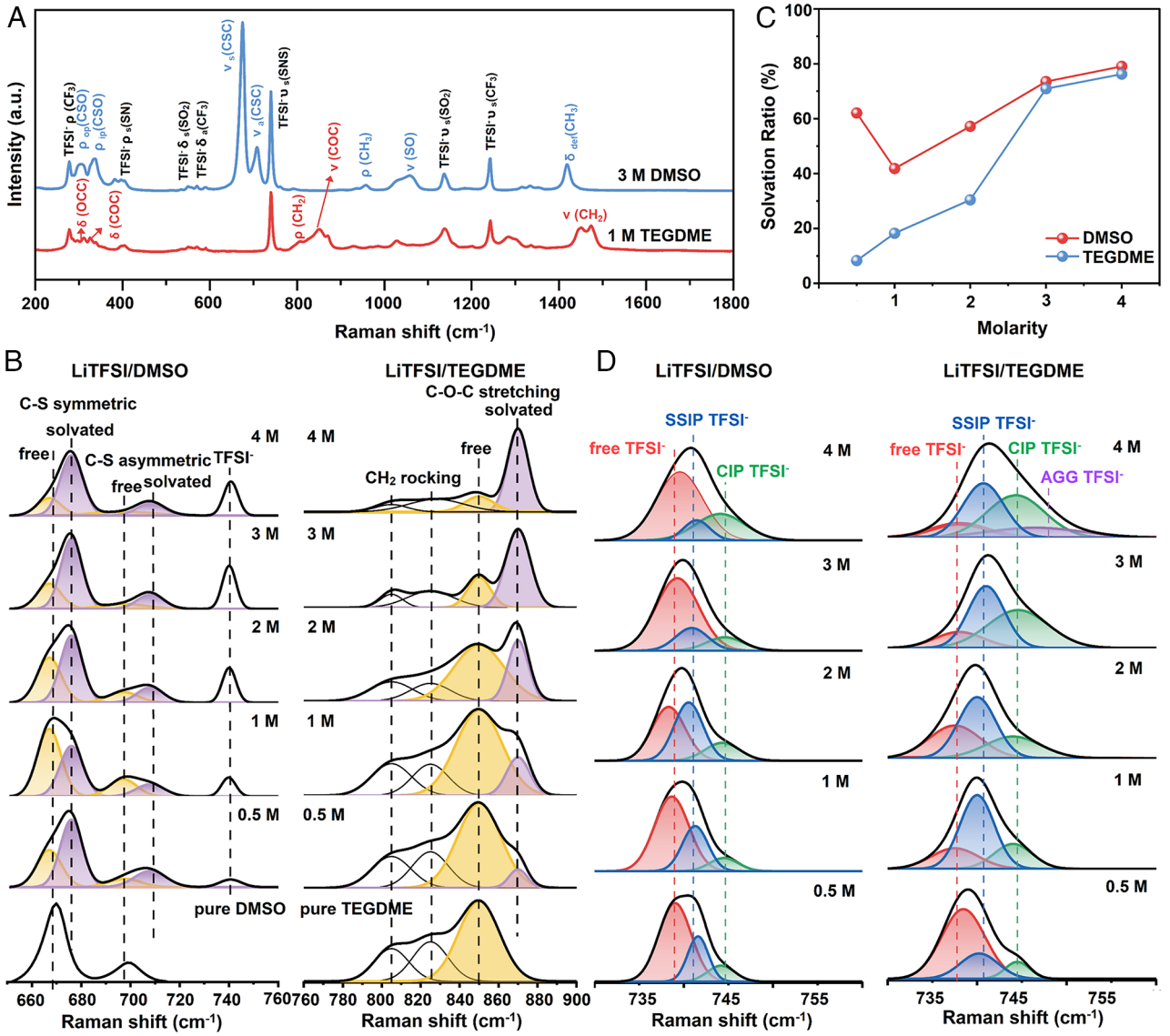

Fig. 3. Raman spectra and acquired solvent solvation ratios of electrolytes with different concentrations. Raman spectra of (*A*) 3 M DMSO and 1 M TEGDME electrolytes in the range of 200 to 1,800 cm^{-1}. (*B*) Raman spectra of DMSO electrolytes in the range of 655 to 760 cm^{-1}, and TEGDME electrolytes in the range of 760 to 900 cm^{-1} with different salt concentrations. (*C*) Solvation ratios of DMSO and TEGDME electrolytes at different salt concentrations. (*D*) Raman spectra of DMSO and TEGDME electrolytes with various salt concentrations in the range of 730 to 760 cm^{-1}.

same salt concentration (*SI Appendix*, Figs. S22 and S23) demonstrate severe Li^+-$TFSI^-$ clustering (revealed by the decreasing free anion percentage) and result in separated mobile Li^+ charge carriers, which are responsible for the slower ion diffusion, lower ionic conductivity, and larger polarization (31–33).

To explain solvation structure–property correlations in depth, radial distribution function (RDF) calculations were conducted to further reveal detailed information on the solvation shell structure, which determines the different SEI formation mechanisms in DMSO- and TEGDME-based electrolytes (34, 35). The bonds of Li–O (DMSO) showed sharp peaks at around 2 Å for all the salt concentrations, while the Li–O bonds (TEGDME) were reflected in weak peaks > 10 Å in 0.5 M TEGDME, demonstrating the stronger solvation energy of DMSO solvent, which is consistent with the Raman results (*SI Appendix*, Figs. S24 and S25). As shown in Fig. 4*A*, it should be noted that the coordination of the O in the $TFSI^-$ anion to the central solvated Li^+ ion [Li–O ($TFSI^-$)] was located at around 2 Å in DMSO-based electrolytes, indicating that $TFSI^-$ anions could access the primary solvation sheath to facilitate the formation of an LiF-rich SEI. In contrast, only 4 M highly concentrated TEGDME electrolyte can be observed to show the existence of $TFSI^-$ near the Li^+ ion in the primary solvation shell based on the peak at 2.05 Å. Under the lower salt concentration in 1 M TEGDME electrolyte (*SI Appendix*, Fig. S26), the peak at around 9.17 Å is far beyond the primary solvation shell of Li^+ ions, indicating that the $TFSI^-$ anions are not involved in the solvation structures in 1M TEGDME electrolyte. When the concentration was increased to 3 M, the Li–O ($TFSI^-$) distance was 2.05 Å in 3 M DMSO electrolyte versus 2.87 Å in 3 M TEGDME electrolyte, demonstrating a stronger interaction between Li^+ and $TFSI^-$ anions in 3 M DMSO electrolyte. The differences in solvation structures explain the higher content of LiF on cathodes cycled in DMSO- than that in TEGDME-based electrolytes: $TFSI^-$ anions participating in primary solvation shells are more likely to react with Li^+ ions after desolvation to generate a robust LiF-rich SEI on the cathode surface, which could effectively protect the cathode from the solvent decomposition and improve the cycling performance (36).

Moreover, DFT calculations were employed to provide more solvation structure information for various concentrated DMSO and TEGDME electrolytes (Fig. 4*B* and *SI Appendix*, Figs. S27 and S28). The Gibbs free energy change results show that with a 3 M LiTFSI concentration, a single Li^+ ion is prone to bond with five DMSO molecules to form stable structures of Li $(DMSO)_5^+$, while just two TEGDME molecules combine with an Li^+ ion to form Li $(TEGDME)_2^+$, indicating that there are less free solvent molecules in DMSO- than those in TEGDME-based electrolytes, and thus, less side reaction products from solvent decomposition (Fig. 4 *C* and *D* and *SI Appendix*, Table S2). Based on DFT calculations, $TFSI^-$ anions can each be connected to two Li^+ ions to form representative $Li^+(TFSI^-)_2$ complexes in 3 M DMSO solution, which contributes to forming the LiF-rich SEI. The above RDF calculation results confirm that more $TFSI^-$ anions are coordinated to the solvated Li^+ ions in the first solvation shells in DMSO than those in TEGDME electrolytes. The DMSO with a high Gutmann's DN (29.8 kcal mol^{-1}) and TEGDME with a low DN (16.6 kcal mol^{-1}) lead to not only different solvation structures in electrolytes, but also distinct reaction kinetics via the solvent reaction pathway. The solvated Li^+ is dominant in DMSO electrolytes as a strong solvent, which could effectively suppress side reactions from solvent decomposition. In contrast, severe side reactions could be observed because of the existence of abundant free

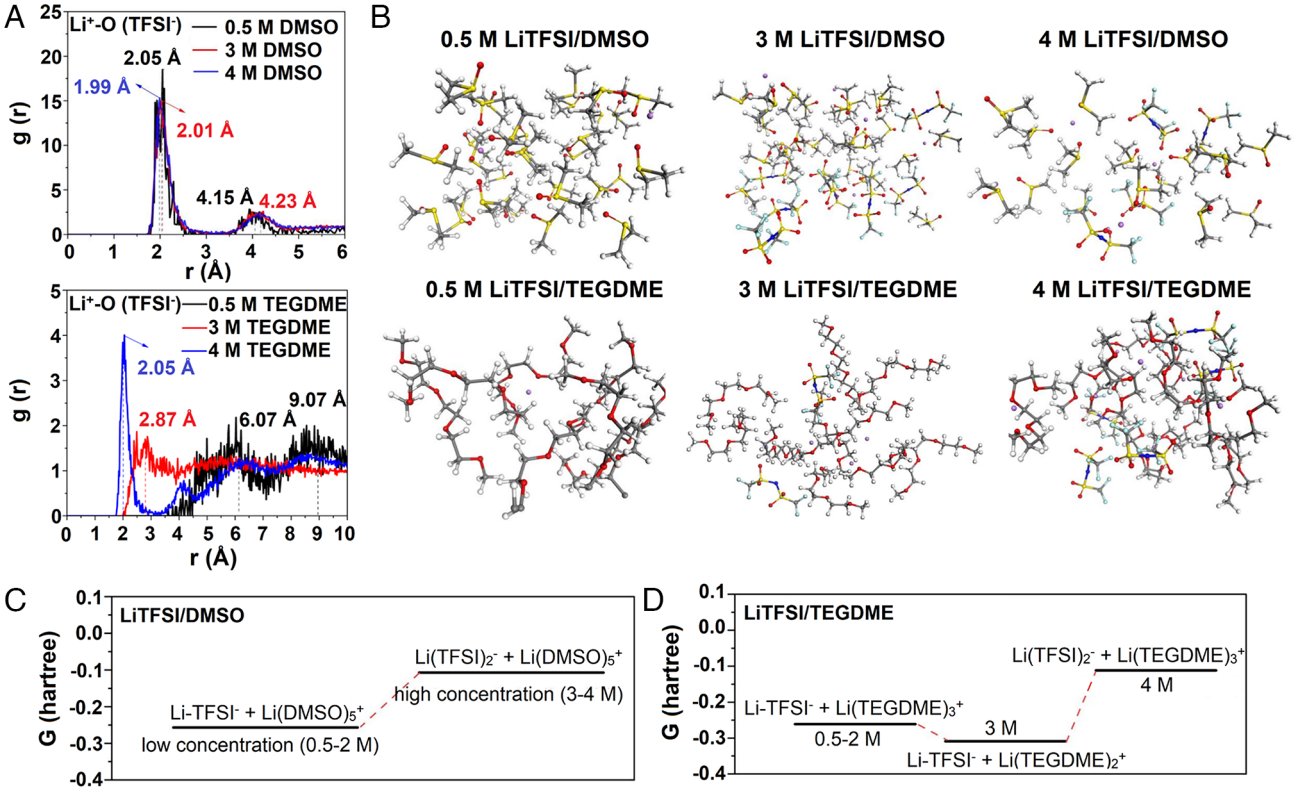

Fig. 4. RDF and DFT calculations of the solvation structures of the electrolytes. (*A*) RDF of Li^+ with respect to the oxygen from the $TFSI^-$ anion at different salt concentrations of DMSO- and TEGDME-based electrolytes; (*B*) DFT-MD simulations from the projected density of states of the DMSO and TEGDME electrolytes. Atom color: Li, purple; C, dark gray; H, light gray; O, red; N, blue; S, yellow; F, green. The Gibbs free energy of Li atoms combined with $TFSI^-$ and solvent molecules in the (*C*) DMSO- and (*D*) TEGDME-based electrolytes at different concentrations.

TEGDME solvent molecules in TEGDME electrolytes. In addition, it was observed that severe solvent dehydrogenation and lithium dendrite growth can be greatly suppressed at the electrolyte/Li metal interface in highly concentrated (4 M) DMSO- and TEGDME-based electrolytes due to the greatly decreased free solvent (as shown in *SI Appendix*, Figs. S29 and S30 and Movies S1–S4), which could significantly improve the battery safety by retaining anode stability.

Conclusion

On the basis of our fundamental investigations on the reaction kinetics of aprotic Li-CO_2 electrochemistry, this work has revealed the dynamic formation of the SEI layer on the cathode surface in two commonly used solvent-based electrolytes (DMSO and TEGDME) with various salt concentrations. Employing DMSO-based electrolytes with high DN can effectively reduce the polarization and promote the ion diffusion kinetics. The theoretical simulations further revealed the solvation structure and the related solvated environment of Li^+ ions in these two solvents. The results show that the DMSO favors more $TFSI^-$ anions coordinating with the solvated Li^+ ions in the primary solvation shells than TEGDME. The optimized electrolyte with 3 M LiTFSI in DMSO could facilitate the formation of a robust LiF-rich SEI film on the cathode surface to suppress parasitic side reactions, which enables a fast ion diffusion process and reduction reaction kinetics by regulating the proportion of SSIPs and CIPs structures in the electrolyte. As a result, the cells in 3 M LiTFSI/DMSO electrolyte could deliver excellent cycling performance over 1,900 h (180 cycles). The systematic investigations in this work will deepen our understanding of anions/solvents in the formation of the SEI layer and offer an insightful clue to better interphase design for future electrolyte engineering of Li-CO_2 chemistry.

Materials and Methods

The chemicals, supplier details, preparation procedures of electrolytes, and characterization methods are detailed in *SI Appendix*. The air cathodes were prepared by a filtration process. Typically, 5 mg reduced graphene oxide as catalyst material and 50 μL Nafion solution (~5 wt%) were dispersed in 2 mL ethanol and ultrasonicated for at least 60 min. After that, the suspension was filtered using a Toray carbon paper (TGP-H-060) as a filtering paper. After being dried at 80 °C overnight, the catalysts were uniformly coated on the Toray carbon paper. The catalyst-loaded Toray carbon paper was then punched out into circular sheets with a diameter of 9.5 mm, which were directly used as air cathodes. The Toray carbon paper serves as the gas diffusion layer and current collector for the air cathodes.

For electrochemical tests, CR2032-type coin cells (16 holes on the cathode side) were assembled in an Ar-filled glove box with the air electrodes and lithium chip separated by a glass fiber separator (Whatman, diameter: 19 mm), and the solutions of 0.5 to 4 M LiTFSI in DMSO and TEGDME solvents were used as the electrolytes. The coin cells were sealed in bottles filled with CO_2 for battery tests. The galvanostatic discharge/charge tests were carried out at various current densities with a battery test station (Land, China).

Data, Materials, and Software Availability. All study data are included in the article and/or *SI Appendix*.

ACKNOWLEDGMENTS. Financial support from the National Natural Science Foundation of China (Grant No. 52104315) and the Australian Research Council (LP160101629, DP210101486, and DP200101862) is acknowledged.

Author affiliations: [a]School of Metallurgy and Environment, Central South University, Changsha 410083, China; [b]Chinese National Engineering Research Centre for Control and Treatment of Heavy Metal Pollution, Central South University, Changsha 410083, China; [c]Institute for Superconducting & Electronic Materials, Australian Institute for Innovative Materials, University of Wollongong, Wollongong, New South Wales 2500, Australia; and [d]School of Chemical Engineering and Advanced Materials, The University of Adelaide, Adelaide, South Australis 5005, Australia

1. M. Liu *et al.*, Enhanced electrocatalytic CO_2 reduction via field-induced reagent concentration. *Nature* **537**, 382–386 (2016).
2. H. Li *et al.*, Integrated electromicrobial conversion of CO_2 to higher alcohols. *Science* **335**, 1596–1596 (2012).
3. F. Li *et al.*, Molecular tuning of CO_2-to-ethylene conversion. *Nature* **577**, 509–513 (2020).
4. T. N. Huan *et al.*, Low-cost high-efficiency system for solar-driven conversion of CO_2 to hydrocarbons. *Proc. Natl. Acad. Sci. U.S.A.* **116**, 9735–9740 (2019).
5. Y. Qiao *et al.*, Li-CO_2 electrochemistry: A new strategy for CO_2 fixation and energy storage. *Joule* **1**, 359–370 (2017).
6. W. Zhang, C. Hu, Z. Guo, L. Dai, High-performance K-CO_2 batter-ies based on metal-free carbon electrocatalysts. *Angew. Chem., Int. Ed.* **59**, 3470–3474 (2020).
7. W. Zhang, Y. Liu, Z. Guo, Approaching high-performance potassium-ion batteries via advanced design strategies and engineering. *Sci. Adv.* **5**, 7412 (2019).
8. B. Liu *et al.*, Recent advances in understanding Li-CO_2 electrochemistry. *Energy Environ. Sci.* **12**, 887–922 (2019).
9. F. Ye *et al.*, Topological defect-rich carbon as a metal-free cathode catalyst for high-performance Li-CO_2 batteries. *Adv. Energy Mater.* **11**, 2101390 (2021).
10. J. Zhou *et al.*, Boosting the reaction kinetics in aprotic lithium-carbon dioxide batteries with unconventional phase metal nanomaterials *Proc. Natl. Acad. Sci. U.S.A.* **119**, e2204666119 (2022).
11. C. Yang, K. Guo, D. Yuan, J. Cheng, B. Wang, Unraveling reaction mechanisms of Mo_2C as cathode catalyst in a Li-CO_2 battery. *J. Am. Chem. Soc.* **142**, 6983–6990 (2020).
12. Z. Peng, S. A. Freunberger, Y. Chen, P. G. Bruce, A reversible and higher-rate Li-O_2 battery. *Science* **337**, 563–566 (2012).
13. X. Mu, H. Pan, P. He, H. Zhou, Li-CO_2 and Na-CO_2 batteries: Toward greener and sustainable electrical energy storage. *Adv. Mater.* **32**, 1903790 (2020).
14. S. Sankarasubramanian, J. Kahky, V. Ramani, Tuning anion solvation energetics enhances potassium–oxygen battery performance. *Proc. Natl. Acad. Sci. U.S.A.* **116**, 14899–14904 (2019).
15. Z. Chang *et al.*, Beyond the concentrated electrolyte: Further depleting solvent molecules within a Li^+ solvation sheath to stabilize high-energy-density lithium metal batteries. *Energy Environ. Sci.* **13**, 4122–4131 (2020).
16. L. Johnson *et al.*, The role of LiO_2 solubility in O_2 reduction in aprotic solvents and its consequences for Li-O_2 batteries. *Nat. Chem.* **6**, 1091–1099 (2014).
17. Y. Zhang *et al.*, High-capacity and high-rate discharging of a coenzyme Q_{10}-catalyzed Li-O_2 battery. *Adv. Mater.* **30**, 1705571 (2018).
18. S. Liu *et al.*, An intrinsically non-flammable electrolyte for high-performance potassium batteries. *Angew. Chem. Int. Ed.* **59**, 3638–3644 (2020).
19. J. Chen *et al.*, Electrolyte design for LiF-rich solid-electrolyte interfaces to enable high-performance microsized alloy anodes for batteries. *Nat. Energy* **5**, 386–397 (2020).
20. X. Fu *et al.*, Sulfuryl chloride as a functional additive towards dendrite-free and long-life Li metal anodes. *J. Mater. Chem. A* **7**, 25003–25009 (2019).
21. H. Zhang *et al.*, Designer anion enabling solid-state lithium-sulfur batteries. *Joule* **3**, 1689–1702 (2019).
22. Y. Shang *et al.*, An "Ether-In-Water" Electrolyte boosts stable interfacial chemistry for aqueous lithium-ion batteries. *Adv. Mater.* **32**, 2004017 (2020).
23. H. R. Wang, Y. N. Yang, F. Bai, T. Zhang, Anion-decoordination cell formation process stabilizes dual electrodes for long-life quasi-solid-state lithium metal battery. *Adv. Mater. Interfaces* **9**, 2101840 (2020).
24. S. Liu *et al.*, Manipulating the solvation structure of nonflammable electrolyte and Interface to enable unprecedented stability of graphite anodes beyond 2 years for safe potassium-ion batteries. *Adv. Mater.* **33**, 2006313 (2021).
25. W. Zhang, J. Lu, Z. Guo, Challenges and future perspectives on sodium and potassium ion batteries for grid-scale energy storage. *Mater. Today* **50**, 400–417 (2021).
26. F. Zhang, W. Zhang, D. Wexler, Z. Guo, Recent progress and future advances on aqueous monovalent-ion batteries towards safe and high-power energy storage. *Adv. Mater.* **34**, 2107965 (2022).
27. M. He *et al.*, Concentrated electrolyte for the sodium-oxygen battery: Solvation structure and improved cycle life. *Angew. Chem. Int. Ed.* **55**, 15310–15314 (2016).
28. Y. Ko *et al.*, Liquid-based janus electrolyte for sustainable redox mediation in lithium-oxygen batteries. *Adv. Energy Mater.* **11**, 2102096 (2021).
29. S. Xu *et al.*, Decoupling of ion pairing and ion conduction in ultrahigh-concentration electrolytes enables wide-temperature solid-state batteries. *Energy Environ. Sci.* **15**, 3379–3387 (2022).
30. S. Jiao *et al.*, Stable cycling of high-voltage lithium metal batteries in ether electrolytes. *Nat. Energy.* **3**, 739–746 (2018).
31. T. Liu *et al.*, Ultralight electrolyte for high-energy lithium-sulfur pouch cells. *Angew. Chem. Int. Ed.* **60**, 17547–17555 (2021).
32. Z. Chang *et al.*, A liquid electrolyte with de-solvated lithium ions for lithium-metal battery. *Joule* **4**, 1776–1789 (2020).
33. Z. Yu *et al.*, Rational solvent molecule tuning for high-performance lithium metal battery electrolytes. *Nat. Energy* **7**, 94–106 (2022).
34. J. Holoubek *et al.*, Tailoring electrolyte solvation for Li metal batteries cycled at ultra-low temperature. *Nat. Energy* **6**, 303–313 (2021).
35. Y. Yamada, J. Wang, S. Ko, E. Watanabe, A. Yamada, Advances and issues in developing salt-concentrated battery electrolytes. *Nat. Energy* **4**, 269–280 (2019).
36. X. Ren *et al.*, Role of inner solvation sheath within salt-solvent complexes in tailoring electrode/electrolyte interphases for lithium metal batteries. *Proc. Natl. Acad. Sci. U.S.A.* **117**, 28603–28613 (2022).